



# Convenient synthesis of nanocrystalline powders of phase-pure manganese nitride $\eta$ -Mn<sub>3</sub>N<sub>2</sub>

Mariusz Drygaś<sup>1,\*</sup>, Mirosław M. Bućko<sup>2</sup>, Michał Musiał<sup>1</sup>, and Jerzy F. Janik<sup>1</sup>

<sup>1</sup> Faculty of Energy and Fuels, AGH University of Science and Technology, al. Mickiewicza 30, 30-059 Krakow, Poland

<sup>2</sup> Faculty of Materials Science and Ceramics, AGH University of Science and Technology, al. Mickiewicza 30, 30-059 Krakow, Poland

**Received:** 3 February 2016

**Accepted:** 23 May 2016

**Published online:**

3 June 2016

© Springer Science+Business Media New York 2016

## ABSTRACT

Manganese bis(trimethylsilyl)amide Mn[N(Si(CH<sub>3</sub>)<sub>3</sub>)<sub>2</sub>]<sub>2</sub> was used as a convenient material precursor to prepare pure manganese nitride nanopowders with reaction-controlled average crystallite sizes. The precursor was first reacted with liquid ammonia under reflux conditions and the resulting by-product was pyrolyzed under an ammonia flow at temperatures in the range 150–900 °C. The powder products were characterized mainly by powder X-ray diffraction (XRD) diffraction, SEM/EDX examinations, and FT-IR and micro-Raman spectroscopies. In all cases, a pure phase of nanocrystalline  $\eta$ -Mn<sub>3</sub>N<sub>2</sub> was detected by XRD as the exclusive manganese nitride product. The compound's nanopowders were extremely reactive toward air. Upon oxidation, they formed either MnO for a relatively better crystallized nitride from higher synthesis temperatures or Mn<sub>3</sub>O<sub>4</sub> after self-ignition of a poorly crystalline nitride from a lower synthesis temperature.

## Introduction

Transition metal nitrides are increasingly attractive materials due to their advantageous physical properties including specific structural, optical, electronic, and magnetic features as well as for their potential applications in various fields such as tool and optical coatings or magnetic and sensing devices [1, 2]. One group of the most appealing materials are various manganese nitrides with unique and diverse magnetic properties [3–5]. The magnetic properties, which could potentially allow for the formation of magnetic/nonmagnetic nitride semiconductor structures or ferromagnetic/antiferromagnetic multilayers,

depend on the Mn/N composition ratio which, in turn, effects the nitride crystallographic phase. In the related area, possibility of forming a diluted magnetic semiconductor with a sufficiently high Curie temperature by manganese-doped gallium nitride GaN is crucial in the anticipated spintronics semiconductor materials [6, 7]. In the latter aspect that is of special interest to us, the knowledge of pure reference systems including various magnetic manganese nitrides is prerequisite [8–11] and this was a driving force behind the present study.

There are several manganese nitride phases known in the Mn–N system depending on the temperature range and equilibrium Mn/N ratio [12]. The highest

Address correspondence to E-mail: madrygas@agh.edu.pl

manganese content phase  $\varepsilon$ -Mn<sub>4</sub>N has a regular fcc crystallographic structure. The phase  $\zeta$  that is found for such compositions as Mn<sub>5</sub>N<sub>2</sub>, Mn<sub>2</sub>N, and Mn<sub>2</sub>N<sub>0.86</sub> shows a hexagonal hcp structure, whereas the phases  $\eta$ -Mn<sub>3</sub>N<sub>2</sub> and  $\theta$ -MnN are tetragonal face centered [5, 14]. These phases have different magnetic properties with the  $\eta$  and  $\theta$  polytypes being antiferromagnetic [3] and  $\varepsilon$  polytype reported to be ferrimagnetic ( $T_c = 738$  K) [15].

In contrast to the rich variety of manganese nitride polytypes, there have been only a handful of reports on the synthesis of the nitride's powders including nanopowders. In this regard, the synthesis has predominantly been accomplished by nitridation of manganese metal in flowing ammonia NH<sub>3</sub> or nitrogen gas N<sub>2</sub>. In this way, for instance, the microcrystalline MnN polytype was synthesized [13]. Reactions of nitrogen or ammonia with Mn-amalgams yielded the  $\eta$  and  $\theta$  manganese nitride phases with no reference to their crystallinity [16]. High-energy ball-milled manganese metal when nitrided with N<sub>2</sub> at 823–1023 K resulted in Mn<sub>4</sub>N and Mn<sub>2</sub>N<sub>0.86</sub> [5]. Microwave energy was used to produce mixtures of Mn<sub>2</sub>N and Mn<sub>4</sub>N using metallic Mn and N<sub>2</sub>/H<sub>2</sub> as precursor systems [17]. Two more ways described in the literature include high-pressure autoclave methods [18]. In the first approach, MnI<sub>2</sub> and NaNH<sub>2</sub> were reacted with ammonia at 6 kbar in the temperature range 400–600 °C to yield microcrystalline nitride Mn<sub>6</sub>N<sub>5</sub>. In the second synthesis, an autoclave-synthesized precursor Na<sub>2</sub>[Mn(NH<sub>2</sub>)<sub>4</sub>] was decomposed at 500 °C to afford microcrystalline  $\eta$ -Mn<sub>3</sub>N<sub>2</sub>.

Polycrystalline films of Mn<sub>8</sub>N<sub>5.32</sub> composition were produced by nitridation of Mn films with NH<sub>3</sub> at 300 °C [19]. Thin films were also made by RF MBE synthesis on a MgO substrate; depending on synthesis conditions either  $\eta$ -Mn<sub>3</sub>N<sub>2</sub> [20] or  $\theta$ -MnN [21] were obtained. Reactive sputtering of the Mn-disc in the Ar/N<sub>2</sub> mixture produced MnN that decomposed to Mn<sub>3</sub>N<sub>2</sub> at 758 K [22]. Low-temperature CVD processing in the system bis(di(tert-butyl)amido)manganese(II) and ammonia afforded thin films of mixed-phase manganese polytypes including  $\eta$ -Mn<sub>3</sub>N<sub>2</sub> [23]. Mn<sub>3</sub>N<sub>2</sub> was also synthesized by high-pressure (10 GPa) and high-temperature (1800 K) reactions of elemental Mn and N<sub>2</sub> [24].

There are scarce literature reports known to us for the preparation of nanocrystalline manganese nitrides [20]. One of the methods utilizes high-

pressure autoclave reactions in the system MnCl<sub>2</sub>/NaN<sub>3</sub>/toluene at 290 °C. The powders of pure  $\theta$ -MnN or of a mixture of  $\eta$ -Mn<sub>3</sub>N<sub>2</sub> and  $\varepsilon$ -Mn<sub>4</sub>N are synthesized with average crystallite sizes of in the range of 20 nm [25]. Phase-pure nanocrystalline  $\eta$ -Mn<sub>3</sub>N<sub>2</sub> powders with average crystallite sizes of several tens of nanometers are actually claimed only in one system, namely, MnCl<sub>2</sub> + LiNH<sub>2</sub>, employing either the solid-state reactions [26] or solvothermal synthesis conditions [27].

Herein, reported is a study on a convenient synthesis route to powders of the rare nanocrystalline manganese nitride  $\eta$ -Mn<sub>3</sub>N<sub>2</sub> with reaction-controlled average crystallite size. The known manganese bis(trimethylsilyl)amide Mn[N(Si(CH<sub>3</sub>)<sub>3</sub>)<sub>2</sub>]<sub>2</sub> was used as the material precursor in the system with ammonia. A similar ammonolysis system has been tried in the past; however, only a sketchy account of plausible manganese products was given based merely on thermogravimetry under helium of a by-product from ammonolysis and on theoretical speculations involving the Mn–N phase diagram [28]. In our hands, this compound was first reacted with liquid ammonia under reflux conditions. After partial ammonolysis/transamination, a resulting by-product powder was pyrolyzed at various temperatures under an ammonia flow to afford final products. The latter were examined mainly with powder X-ray diffraction (XRD) and scanning electron microscopy SEM/EDX. Infrared spectroscopy FT-IR was used both to control model precursor reactions and to characterize final products. Micro-Raman spectroscopy was applied, mainly, to check for potential carbon impurities. Due to the extremely high affinity of nanopowders to oxidation no magnetization data could be acquired.

## Experimental

All reactions were performed using standard Schlenk techniques under an inert atmosphere of argon gas or under vacuum. The solvents were rigorously dried before reactions, operations with by-products and final powders were routinely carried out in a dry box.

In the first step, manganese bis(trimethylsilyl)amide was synthesized using a modified literature method [29]. Anhydrous manganese chloride MnCl<sub>2</sub> and lithium bis(trimethylsilyl)amide LiN[Si(CH<sub>3</sub>)<sub>3</sub>]<sub>2</sub> were stoichiometrically reacted in

diethyl ether solution. The mixture was stirred overnight and a white precipitate of LiCl was filtered out. After ether/volatiles evacuation, a thick dark brown liquid was obtained. The liquid was distilled under vacuum (ca. 100 mTorr) at 100–110 °C. The distillate solidified in a form of pale pink crystallites of  $\text{Mn}[\text{N}(\text{Si}(\text{CH}_3)_3)_2]_2$ . Typically, the batch was further purified by a second distillation. The resulting compound had a melting point of 56–58 °C.

In the second step, a few millimoles of the compound reacted for 4 h with a large excess of liquid ammonia  $\text{NH}_3$  (ca. 50–60 ml) under reflux conditions. Following ammonia removal and 30-min volatiles evacuation at room temperature, a cream-colored fine powder was obtained. Typically, 74 wt% mass losses were recorded at this stage. Subsequently, the powder was placed into a quartz reactor and pyrolyzed under an ammonia flow ( $1 \text{ cm}^3/\text{s}$ ) for 4 h at a selected temperature in the range 300–900 °C. Two samples were individually prepared in a Schlenk flask by pyrolysis at 150 and 200 °C, 18 h, under an ammonia flow using a silicone oil bath. In all cases and independent on pyrolysis temperature, 34 wt% mass losses were experienced which was consistent with complete nitridation taking place already at the lowest temperature of 150 °C (vide infra). All product powders had a brown-black to black color. Summary of the preparation steps is shown in Fig. 1.

Some model reactions of  $\text{Mn}[\text{N}(\text{Si}(\text{CH}_3)_3)_2]_2$  with measured amounts of ammonia gas were also performed on a small scale at room temperature to get insight into the nature of all ammonolysis products.

All product powders were characterized by the standard powder XRD technique with a X'Pert Pro Panalytical diffractometer (Cu  $K_\alpha$  source;  $2\theta = 20^\circ$ –

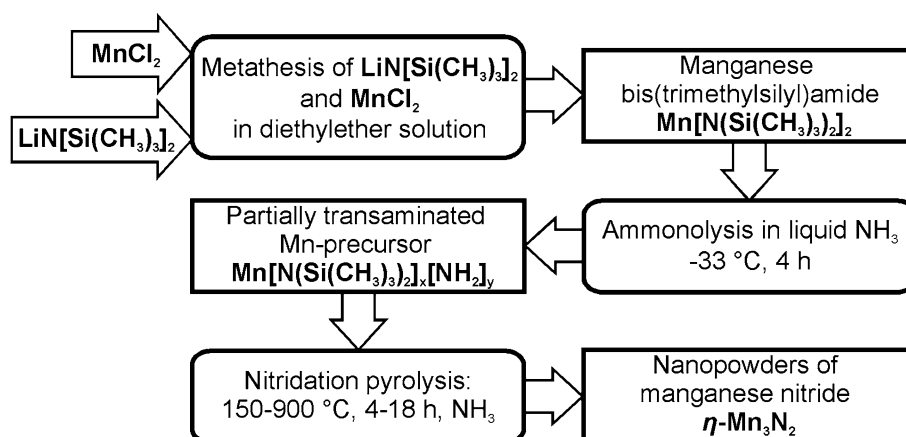
80°), FT-IR patterns for solids (KBr pellets) and gas samples were collected on a Nicolet 380 spectrometer, SEM/EDX measurements were done using a Hitachi Model S-4700 scanning electron microscope, and micro-Raman analysis for a product sealed under vacuum in a glass vial was carried out by HORIBA LabRAM HR spectrometer equipped with 532 nm laser. In order to minimize product oxidation during XRD determinations, the powders were typically mixed with a small amount of paraffin oil to form thick pastes.

## Results and discussion

The anticipated reaction chemistry in the system involves, first, a plausible ammonia-mediated transamination according to an idealized reaction  $\text{Mn}[\text{N}(\text{Si}(\text{CH}_3)_3)_2]_2 + \uparrow 2\text{NH}_3 \rightarrow \text{Mn}(\text{NH}_2)_2 + \uparrow 2\text{HN}[\text{Si}(\text{CH}_3)_3]_2$  (volatile hexamethyldisilazane). And second, thermally driven deamination of the transient Mn-amide should conveniently yield the respective nitride from a stepwise reaction sequence such as  $3\text{Mn}(\text{NH}_2)_2$  (amide)  $\rightarrow$   $3\text{Mn}(\text{NH})$  (imide)  $+$   $\uparrow 3\text{NH}_3 \rightarrow \text{Mn}_3\text{N}_2$  (nitride)  $+$   $\uparrow \text{NH}_3$ .

In this regard, there are two somewhat incoherent studies known to us claiming the preparation of manganese amide  $\text{Mn}(\text{NH}_2)_2$ . In the first report, autoclave reactions of manganese metal with supercritical ammonia (100 bar, 130 °C, 10 days) in the presence of a mineralizer apparently yielded the ruby-red amide of which crystal structure was solved [30]. The second report claimed the preparation of impure (potassium contaminated) light yellow  $\text{Mn}(\text{NH}_2)_2$  from the metathetical reaction of

**Figure 1** Experimental scheme for the preparation of nanocrystalline powders of manganese nitride  $\eta\text{-Mn}_3\text{N}_2$ .



potassium amide  $\text{KNH}_2$  and manganese thiocyanate  $\text{Mn}(\text{SCN})_2$  [31]; in that paper, heating of the manganese amide at some  $120^\circ\text{C}$  was postulated to yield a poorly defined mixture of manganese nitride and manganese imide  $\text{Mn}_2\text{N}_3\cdot\text{MnNH}$ . In the related area, numerous metal (trimethylsilyl)amides  $\text{M}[\text{N}(\text{Si}(\text{CH}_3)_3)_2]_n$ ,  $\text{M}$  = metal, upon reactions with ammonia have been useful precursors to metal nitride nanoparticles via thermal decomposition/deamination of the postulated metal amides  $\text{M}(\text{NH}_2)_n$  as outlined in a recent review [32]. Analogous chemistry was also successfully explored by some of us to prepare nanocrystalline powders of gallium nitride  $\text{GaN}$  [33–35], aluminum nitride  $\text{AlN}$  [36, 37], and titanium nitride  $\text{TiN}$  [38, 39] from transamination with ammonia of, respectively, gallium tris(dimethyl)amide  $\text{Ga}[\text{N}(\text{CH}_3)_2]_3$ , aluminum tris(dimethyl)amide  $\text{Al}[\text{N}(\text{CH}_3)_2]_3$ , and titanium tetrakis(dimethyl)amide  $\text{Ti}[\text{N}(\text{CH}_3)_2]_4$ . In this regard, the related manganese bis(dimethyl)amide  $\text{Mn}[\text{N}(\text{CH}_3)_2]_2$  has not been reported to date and our initial attempts to make it via transamination with dimethylamine of  $\text{Mn}[\text{N}(\text{Si}(\text{CH}_3)_3)_2]_2$  have so far missed the target. It is worth to mention that a related bulky bis[di(tert-butyl)amido]manganese(II),  $\text{Mn}[\text{N}(\text{t-Bu})_2]_2$ , in the system with ammonia was successfully used to make thin films of mixed-phase manganese nitrides, possibly, via transamination and subsequent deamination reactions of the transient manganese amide/imide [23]. The  $\text{Mn}[\text{N}(\text{Si}(\text{CH}_3)_3)_2]_2$  itself was applied as a volatile precursor for deposition of thin films of metallic manganese [40–42]. In summary of this aspect, the grounds for the transamination/deamination chemistry in the system  $\text{Mn}[\text{N}(\text{Si}(\text{CH}_3)_3)_2]_2/\text{NH}_3$  leading to manganese nitride are solid and well substantiated.

The FT-IR spectrum of  $\text{Mn}[\text{N}(\text{Si}(\text{CH}_3)_3)_2]_2$  is shown in Fig. 2. It displays the C–H stretching bands in the  $\text{CH}_3$  groups at  $2960$  and  $2890\text{ cm}^{-1}$ , and the strong bands at  $1250$ ,  $930$ , and  $840\text{ cm}^{-1}$ , which can be linked to various vibrational modes in the  $\text{N}(\text{Si}(\text{CH}_3)_3)_2$  group.

The ammonolysis of manganese bis(trimethylsilyl)amide was first performed in a 100-ml evacuated flask with 1 mmol of compound onto which 4 mmol of ammonia were transferred at liquid nitrogen temperature. Upon warming up to room temperature, the flask was maintained for 0.5 h at ambient and both the volatiles and the solid product were examined with FT-IR spectroscopy. A strong

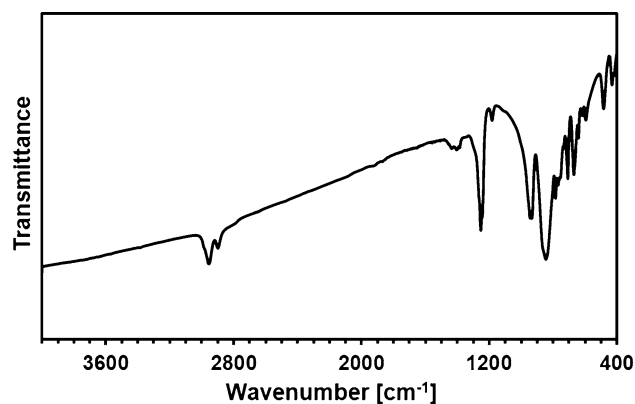


**Figure 2** FT-IR spectrum of manganese bis(trimethylsilyl)amide  $\text{Mn}[\text{N}(\text{Si}(\text{CH}_3)_3)_2]_2$ .

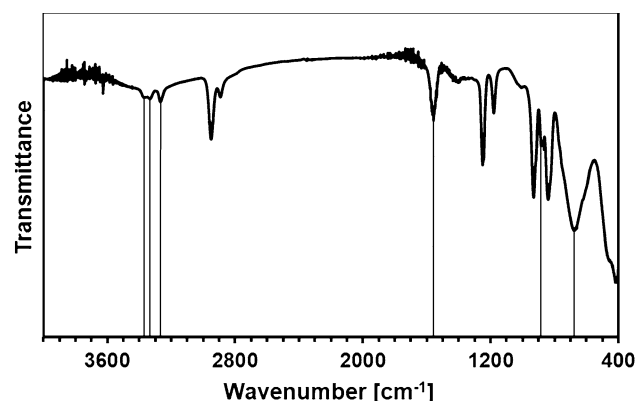


**Figure 3** FT-IR spectrum of the solid product from reactions of manganese bis(trimethylsilyl)amide with large excess of ammonia. Vertical lines drawn for the characteristic N–H vibrations in  $\text{NH}_2$ -amide groups are guides to the eye, only.

evidence for ammonolysis of  $\text{Mn}[\text{N}(\text{Si}(\text{CH}_3)_3)_2]_2$  was detection of hexamethyldisilazane  $\text{HN}[\text{Si}(\text{CH}_3)_3]_2$ , the expected ammonolysis by-product, which was accompanied by some unreacted excess ammonia in the gaseous reaction products (not shown).

The FT-IR spectrum for the solid from this reaction matched the spectrum for a solid product from the reaction of the amide with large excess of ammonia under reflux conditions (Fig. 3). The three weak bands at ca.  $3330$ ,  $3370$ , and  $3270\text{ cm}^{-1}$  and the band at  $1560\text{ cm}^{-1}$  can be assigned to the N–H stretching and deformation modes in the  $\text{NH}_2$ -amide groups, respectively, whereas the broadbands at  $680$  and  $890\text{ cm}^{-1}$  are the N–H wagging modes in these groups [43]. There is a strong and broad band in the vicinity of  $400\text{ cm}^{-1}$ , which extends toward lower wavenumbers, and which can possibly be associated

with Mn–N vibrations outside the mid-infrared range. The remaining bands can be assigned to residual/unreacted  $\text{N}(\text{Si}(\text{CH}_3)_3)_2$  groups in the by-product. Based on these assignments, the solid obtained from ammonolysis is thought to have an approximate composition  $[\text{Mn}[\text{N}(\text{Si}(\text{CH}_3)_3)_2]_x(\text{NH}_2)_y]_n$  resulting from merely partial transamination. It is instructive to note that the recorded mass loss during the ammonolysis stage of the order of 74 wt% corresponds with  $x = 0.07$  and  $y = 1.93$  in the formula to be

compared with the theoretical 76.8 wt% loss for the complete transamination and the formation of  $\text{Mn}(\text{NH}_2)_2$  end-product. The highly associated structure of the solid, which is not soluble in any of the common organic solvents, could likely be formed via N-donor to Mn-acceptor bonding in the tight framework of the type  $\{-[\text{N}(\text{Si}(\text{CH}_3)_3)_2]_2\text{-Mn}-(\text{H}_2)\text{N} \rightarrow \text{Mn}-[\text{N}(\text{Si}(\text{CH}_3)_3)_2]-\text{N}(\text{H}_2) \rightarrow \text{Mn}-\}_n$ . In conclusion, all the experimental evidence is consistent with an incomplete alas deep transamination of  $\text{Mn}[\text{N}(\text{Si}(\text{CH}_3)_3)_2]_2$  under

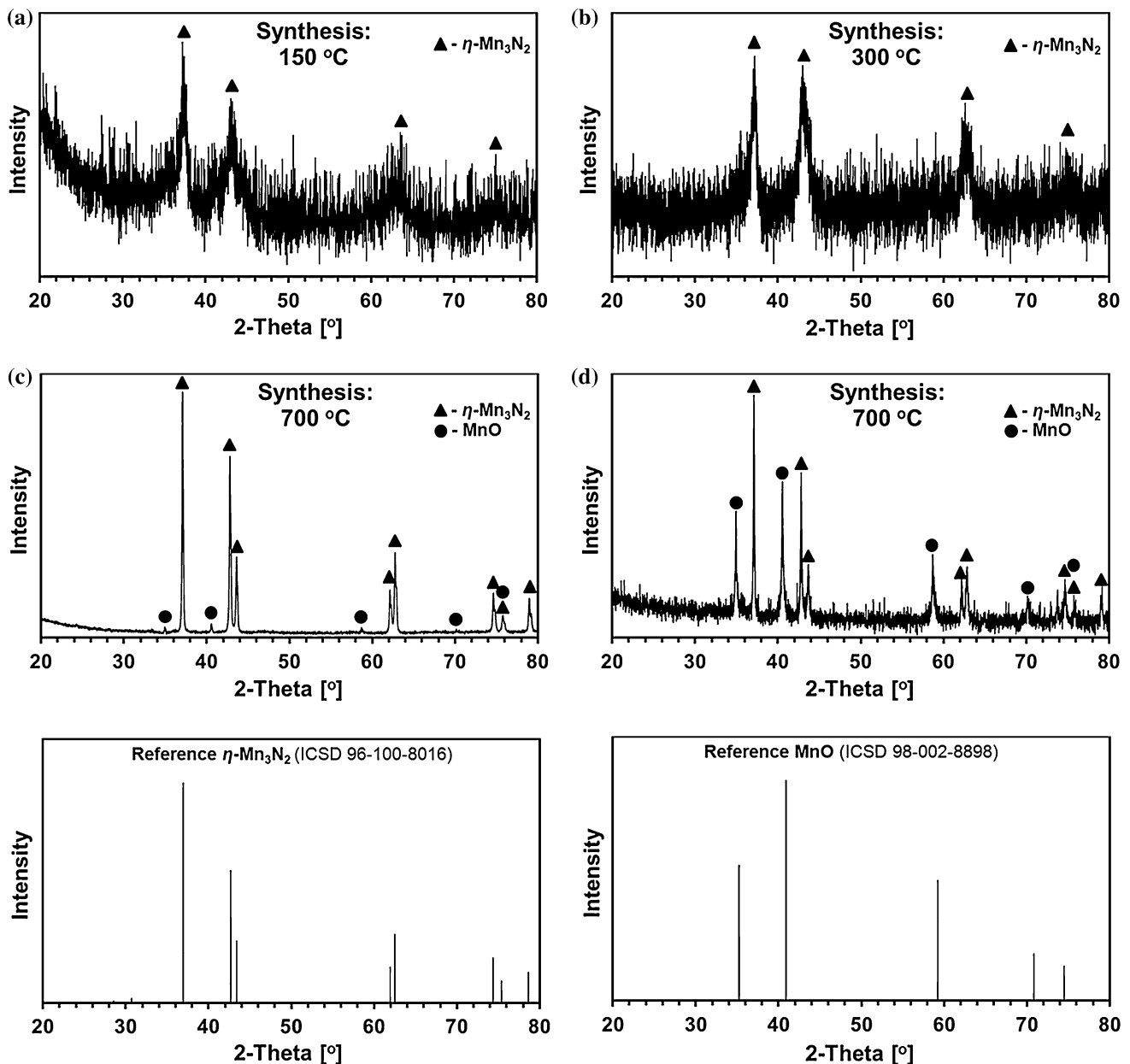


**Figure 4** XRD patterns obtained for samples/pastes made with a protective hydrocarbon oil a–c and for unprotected bulk powder sample d. Bottom row shows the reference bar charts for  $\eta\text{-Mn}_3\text{N}_2$  (left) and  $\text{MnO}$  (right).

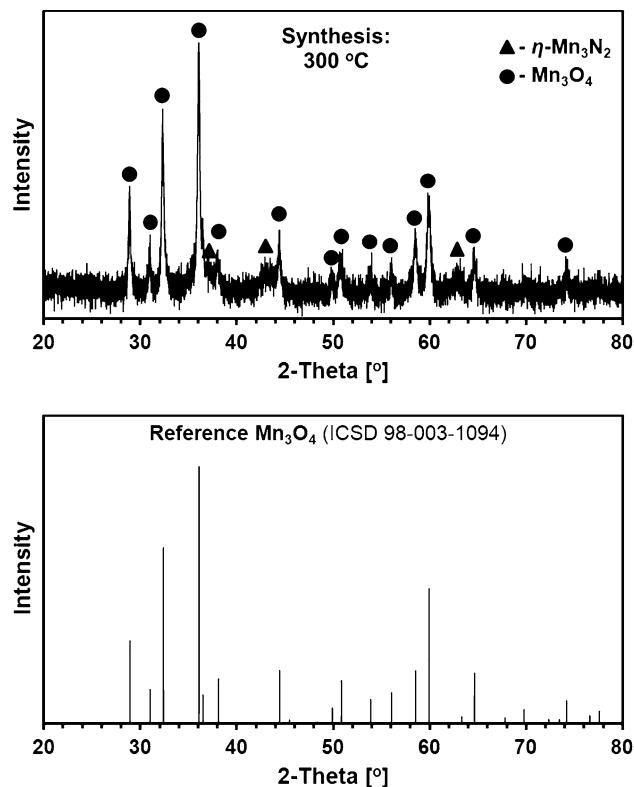
the applied conditions and the resulting precursor still containing some residual  $\text{N}(\text{Si}(\text{CH}_3)_3)_2$  groups.

The XRD patterns for the products from pyrolysis at 150, 300, and 700 °C that were run carefully for paste samples made with powders and mineral oil are shown in Fig. 4. Their major features can be indexed as a tetragonal phase of  $\eta\text{-Mn}_3\text{N}_2$ . For the lowest temperature products, the broad peaks are indicative of extremely small average crystallite sizes. For the 700 °C-product, a small and moderate quantity of manganese oxide  $\text{MnO}$  for the oil-protected and unprotected powders, respectively, are additionally detected, which we attribute to incidental partial oxidation during sample handling and measurements (*cf.* Fig 4c, d). Actually, the 300 °C-powder self-ignited during the measurement, which was evidenced by an evolving smoke. The determination and data work-up were carried out anyway resulting in the major component  $\text{Mn}_3\text{O}_4$  and a small quantity of the remaining  $\eta\text{-Mn}_3\text{N}_2$  (Fig. 5). This was the only time that  $\text{Mn}_3\text{O}_4$  was detected as the nitride's oxidation product with  $\text{MnO}$  being encountered in all other cases, instead; apparently, the former oxide is synthesized under conditions of a very reactive product from lower temperature synthesis and ample oxygen available from air.

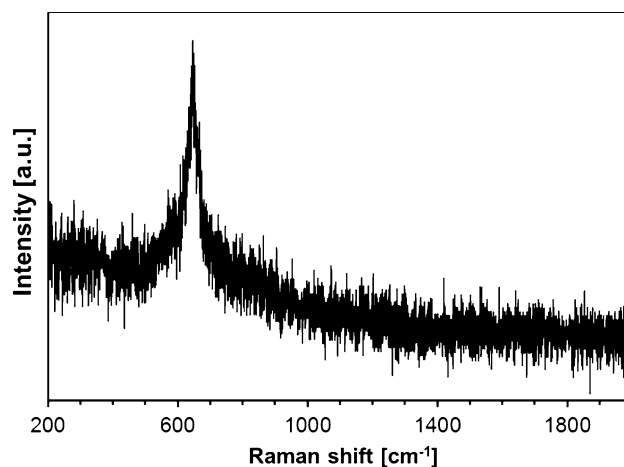
The FT-IR spectra for the powder products in KBr pellets (prepared under anaerobic conditions in dry-box) showed no essential absorption bands in the 400–4000  $\text{cm}^{-1}$  range. This supports no Mn–N vibrations in the mid-infrared range and conforms with the lack of well-substantiated information of this kind for manganese nitrides to date [44]. Interestingly, a micro-Raman spectrum obtained for the 300 °C-nitrided sample that was sealed under vacuum in a glass vial displayed a single strong band at ca. 640  $\text{cm}^{-1}$  as shown in Fig. 6.

A similar Raman shift at ca. 650  $\text{cm}^{-1}$  was recently reported for  $\eta\text{-Mn}_3\text{N}_2$  with much greater average crystallite sizes (>50 nm vs. 8.5 nm in this study) [27]; the size characteristics explains the broadness of the peak in Fig. 6. It is to be noted, too, that there is no evidence in the spectrum for the presence of impurities, especially, there are no bands in the range 1300–1600  $\text{cm}^{-1}$ , which are typical for various forms of free carbon. The latter could theoretically be formed from thermal cracking of residual  $\text{N}(\text{Si}(\text{CH}_3)_3)_2$  groups, if any.

The crystallographic parameters of the nitride including average crystallite sizes calculated from Scherrer equation are included in Table 1. It is worth noting that all products consisted exclusively of one



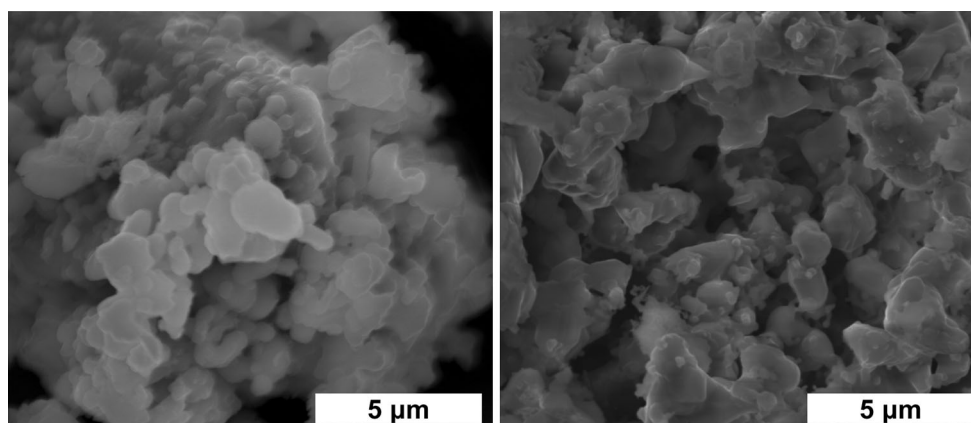
**Figure 5** XRD pattern obtained for unprotected powder from the 300 °C-synthesis after self-ignition in air. Bar chart in the *bottom* is for the reference  $\text{Mn}_3\text{O}_4$ .



**Figure 6** Micro-Raman spectrum for sealed powder from the 300 °C-synthesis.

**Table 1** Crystallographic parameters of  $\eta$ -Mn<sub>3</sub>N<sub>2</sub> in product nanopowders

Product characteristics (pyrolysis conds.; sample)	Crystallographic phase(s)	Lattice constants for tetragonal $\eta$ -Mn <sub>3</sub> N <sub>2</sub> (Å)	Av. crystallite size of $\eta$ -Mn <sub>3</sub> N <sub>2</sub> (nm)
150 °C, 18 h; oil paste	$\eta$ -Mn <sub>3</sub> N <sub>2</sub>	$a = 2.97$ $c = 12.28$	4
200 °C, 18 h; oil paste	$\eta$ -Mn <sub>3</sub> N <sub>2</sub>	$a = 2.97$ $c = 12.35$	5
300 °C, 4 h; oil paste	$\eta$ -Mn <sub>3</sub> N <sub>2</sub>	$a = 2.95$ $c = 12.65$	8.5
300 °C, 4 h; powder (after self-ignition)	$\eta$ -Mn <sub>3</sub> N <sub>2</sub> , 24 % (Mn <sub>3</sub> O <sub>4</sub> , 76 %)	$n/d$	n/d
500 °C, 4 h; powder	$\eta$ -Mn <sub>3</sub> N <sub>2</sub> , 62 % (MnO, 38 %)	$a = 2.98$ $c = 12.45$	25
700 °C, 4 h; powder	$\eta$ -Mn <sub>3</sub> N <sub>2</sub> , 54 % (MnO, 46 %)	$a = 2.98$ $c = 12.42$	76
700 °C, 4 h; oil paste	$\eta$ -Mn <sub>3</sub> N <sub>2</sub> , 98 % (MnO, 2 %)	$a = 2.99$ $c = 12.45$	95
900 °C, 4 h; oil paste	$\eta$ -Mn <sub>3</sub> N <sub>2</sub> , 43 % (MnO, 57 %)	$a = 2.98$ $c = 12.37$	>200

**Figure 7** SEM images of products prepared at 300 °C (left) and 900 °C (right).

manganese nitride, i.e., tetragonal  $\eta$ -Mn<sub>3</sub>N<sub>2</sub>. In this regard, the phase diagram and other literature data [3, 13] suggest  $\theta$ -MnN to be stable at temperatures below 480 °C. Above that temperature and under vacuum, it decomposes to  $\eta$ -Mn<sub>3</sub>N<sub>2</sub> which, under such conditions, shows an apparent stability up to ca. 620 °C. At this point, it converts to the phase  $\zeta$  (Mn<sub>5</sub>N<sub>2</sub>, Mn<sub>2</sub>N, Mn<sub>2</sub>N<sub>0.86</sub>) and at temperatures higher than ca. 760 °C the  $\varepsilon$ -Mn<sub>4</sub>N phase should be preferred. In contrast to these findings, under the conditions employed in our experiments the nanocrystalline  $\eta$ -Mn<sub>3</sub>N<sub>2</sub> phase seems to be a stable polytype from 150 up to 900 °C.

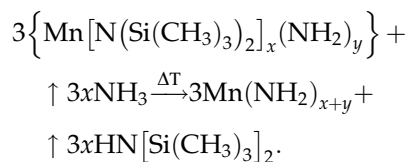
It needs to be stressed that the synthesis affords average crystallite sizes ranging from a few to more than 200 nm being controlled simply by pyrolysis

temperature. To the best of our knowledge, this is the first time that crystallite sizes of  $\eta$ -Mn<sub>3</sub>N<sub>2</sub> are reported in the low nanosized regime. The other two cases known to us for the synthesis of the phase-pure nitride, both in the system MnCl<sub>2</sub> + LiNH<sub>2</sub>, yielded much larger sizes of 20–30 nm (solid state reactions [26]) or above 50 nm (solvothermal synthesis [27]).

SEM images show rather irregular particle morphology for all products and the particles appear to form fused aggregates (Fig. 7). The higher is the pyrolysis temperature, the particles assume more and more individual/separated shapes. The EDX microanalyses for the powders synthesized in the temperature range 500–900 °C indicate increasing nitrogen to oxygen ratios with the increasing pyrolysis temperature, i.e., N/O atomic ratios from 0.2 to 0.7,

respectively, which is consistent with a relatively lower propensity for post-synthesis oxidation of the then larger and larger nitride crystallites. We want to stress that the surface sensitive EDX analysis reflects compositions on oxidized particle surfaces and, therefore, overestimates oxygen contents. However, the N/O ratio trend is qualitatively significant. As previously indicated, the extremely high susceptibility for oxidation prevented us from standard measurements of the nitride's magnetic properties.

The formation of the pure  $\eta$ -Mn<sub>3</sub>N<sub>2</sub> is consistent with efficient ammonolysis of the room temperature-isolated precursor during its nitridation pyrolysis at 150–900 °C (Fig. 1). The major reactions in this final step could be described by the idealized equations shown below.



Since  $x = 0.07$ ,  $y = 1.93$ , and  $x + y = 2$ , then  $3\text{Mn}\left(\text{NH}_2\right)_2 \xrightarrow{\Delta T} \text{Mn}_3\text{N}_2 + \uparrow 4\text{NH}_3$ .

In the initial stages of pyrolysis of the partially transaminated precursor, transamination with ammonia is completed and results in removing the remnant N(Si(CH<sub>3</sub>)<sub>3</sub>)<sub>2</sub> groups by forming the volatile hexamethyldisilazane HN[Si(CH<sub>3</sub>)<sub>3</sub>]<sub>2</sub>, whereas the assumed transient manganese amide decomposes via deamination of the manganese nitride. As the consequence of abundance of nitrogen (from ammonia) and reducing conditions, no change in the formal oxidation state of manganese (II) occurs and the formation of the N-rich  $\eta$ -Mn<sub>3</sub>N<sub>2</sub> polytype takes place.

The observed at this final stage mass loss of 34 wt%, which is independent on pyrolysis temperature, supports an efficient ammonolysis of the residual N(Si(CH<sub>3</sub>)<sub>3</sub>)<sub>2</sub> groups followed by deamination of the resulting Mn(NH<sub>2</sub>)<sub>2</sub> all to take place already at 150 °C or lower. This experimental mass loss can be compared with the theoretical mass loss of 33.8 wt% calculated for the above reactions with  $x = 0.07$  and  $y = 1.93$ . The remarkable agreement of these two values supports high purity of the nitride product. In this regard, the EDX analyses showed some Si-content on the verge of detection only for the 150 °C-product, whereas no Si was detected for products from the higher pyrolysis temperatures. Similarly, the

Raman data showed no free C-contents as yet another possible contamination while supporting one nitride product. In conclusion, therefore, all by-products are efficiently removed as volatiles from the system affording exclusively  $\eta$ -Mn<sub>3</sub>N<sub>2</sub> of substantial purity.

## Conclusions

Convenient preparation of the nanocrystalline powders of pure manganese nitride  $\eta$ -Mn<sub>3</sub>N<sub>2</sub> is demonstrated. The rare nitride is obtained via transamination/deamination reactions in the precursor system Mn[N(Si(CH<sub>3</sub>)<sub>3</sub>)<sub>2</sub>]<sub>2</sub>/NH<sub>3</sub>. The transamination process is not complete at room temperature but further pyrolysis under ammonia at 150–900 °C completes it and upon subsequent deamination yields the exclusive nitride  $\eta$ -Mn<sub>3</sub>N<sub>2</sub>. The average crystallite size strongly depends on pyrolysis temperature ranging from 4 nm (150 °C) to over 200 nm (900 °C). The nanopowders are agglomerated and have irregular morphology; at the highest pyrolysis temperatures, the particles appear to be relatively more separated from each other. The pure nanopowders of  $\eta$ -Mn<sub>3</sub>N<sub>2</sub> are highly reactive in air and if not protected quickly form manganese oxides MnO or Mn<sub>3</sub>O<sub>4</sub>.

## Acknowledgements

The study was supported by Polish NCN Grant 2011/01/B/ST5/06592.

## References

- [1] Gall D, Petrov I, Desjardins P, Greene JE (1999) Microstructural evolution and Poisson ratio of epitaxial ScN grown on TiN(001)/MgO(001) by ultrahigh vacuum reactive magnetron sputter deposition. *J Appl Phys* 86:5524–5529
- [2] Smith AR, Al-Britthen HAH, Ingram DC, Gall D (2001) Molecular beam epitaxy control of the structural, optical, and electronic properties of ScN(001). *J Appl Phys* 90:1809–1816
- [3] Suzuki K, Kaneko T, Yoshida H, Obi Y, Fujimori H, Morita H (2000) Crystal structure and magnetic properties of the compound MnN. *J Alloy Compd* 306:66–71
- [4] Leineweber A, Niewa R, Jacobs H, Kockelmann W (2000) The manganese nitrides  $\eta$ -Mn<sub>3</sub>N<sub>2</sub> and  $\theta$ -Mn<sub>6</sub>N<sub>5</sub> + x: nuclear and magnetic structures. *J Mater Chem* 10:2827–2834

- [5] Feng WJ, Sun NK, Du J, Zhang Q, Liu XG, Deng YF, Zhang ZD (2008) Structural evolution and magnetic properties of Mn–N compounds. *Sol State Commun* 148:199–202
- [6] Ohno H (1998) Making nonmagnetic semiconductors ferromagnetic. *Science* 281:951–955
- [7] Dietl T, Ohno H, Matsukura F, Cibert J, Ferrand D (2000) Zener model description of ferromagnetism in zinc-blende magnetic semiconductors. *Science* 287:1019–1022
- [8] Janik JF, Drygaś M, Czosnek C, Kaminska M, Palczewska M, Paine RT (2004) Carbothermally-assisted aerosol synthesis of semiconducting materials in the system GaN/Mn. *J Phys Chem Sol* 65:639–645
- [9] Gosk JB, Drygaś M, Janik JF, Palczewska M, Paine RT, Twardowski A (2006) Magnetic and optical properties of (GaMn)N nanocrystalline powders prepared by the aerosol-assisted vapour phase synthesis and anaerobic imide route methods. *J Phys D Appl Phys* 39:3717–3725
- [10] Drygas M, Janik JF, Bucko MM, Gosk J, Twardowski A (2015) Structural and magnetic properties of GaN/Mn nanopowders prepared by an anaerobic synthesis route. *RSC Adv* 5:37298–37313
- [11] Drygas M, Janik JF, Gosk J, Gierlotka S, Palosz B, Twardowski A (2016) Structural and magnetic properties of ceramics prepared by high-pressure high-temperature sintering of manganese-doped gallium nitride nanopowders. *J. Eur Ceram. Soc.* 36(1033–1044):14
- [12] Nishiyama Z, Iwanaga R (1945) *Nippon Kinzoku Gakkai-Shi* 9:1
- [13] Gokcen NA (1990) The Mn–N (manganese-nitrogen) system. *Bull Alloy Phase Diagrams* 11:33–42
- [14] Niewa R (2002) Nitridocompounds of manganese: manganese nitrides and nitridomanganates. *Z Kristallogr* 217:8–23
- [15] Takei WJ, Heikes RR, Shirane G (1962) Magnetic structure of  $Mn_4N$ -type compounds. *Phys Rev* 125:1893–1897
- [16] Lihl F, Ettmayer P, Kutzelnigg A (1962) The system manganese-nitrogen. *Z Metallk* 53:715–721
- [17] Huang JW, Li J, Peng H (2007) Microwave synthesis of manganese nitride. *Powder Metall* 50:137–141
- [18] Kreiner G, Jacobs H (1992) Magnetische structure von  $\eta$ - $Mn_3N_2$ . *J Alloy Compd* 183:345–362
- [19] Otsuka N, Hanawa Y, Nagakura S (1977) Crystal structure and phase transition of  $Mn_6N_5$  studied by electron diffraction. *Phys Stat Sol A* 43:127–129
- [20] Yang H, Al-Brithen H, Smith AR, Borchers JA, Cappelletti RL, Vaudin MD (2001) Structural and magnetic properties of h-phase manganese nitride films grown by molecular-beam epitaxy. *Appl Phys Lett* 78:3860–3862
- [21] Yang R, Haider MB, Yang H, Al-Brithen H, Smith AR (2005) Scanning tunneling microscopy study of the structural phase transformation in manganese nitride:  $\theta$ - $MnN \rightarrow \eta$ - $Mn_3N_2$ . *Appl Phys A* 81:695–700
- [22] Suzuki K, Morita H, Kaneko T, Yoshida H, Fujimori H (1993) Crystal structure and magnetic properties of the compound FeN. *J Alloy Compd* 201:11–16
- [23] Spicer TS, Spicer CW, Cloud NA, Davis LM, Girolami GS, Abelson JR (2013) Low-temperature CVD of  $\eta$ - $Mn_3N_2$ - $x$  from bis[di(tert-butyl)amido]manganese(II) and ammonia. *J Vac Sci Technol A* 31:030604
- [24] Hasegawa M, Yagi T (2005) Systematic study of formation and crystal structure of 3d-transition metal nitrides synthesized in a supercritical nitrogen fluid under 10 GPa and 1800 K using diamond anvil cell and YAG laser heating. *J Alloys Compd* 403:131–142
- [25] Choi J, Gillan EG (2009) Solvothermal metal azide decomposition routes to nanocrystalline metastable nickel, iron, and manganese nitrides. *Inorg Chem* 48:4470–4477
- [26] Parkin IP, Rowley AT (1995) Formation of transition-metal nitrides from the reactions of lithium amides and anhydrous transition-metal chlorides. *J Mater Chem* 5:909–912
- [27] Imran S, Shah U, Hector AL, Li XJ, Owen JR (2015) Solvothermal synthesis and electrochemical charge storage assessment of  $Mn_3N_2$ . *J Mater Chem A* 3:3612–3619
- [28] Baxter DV, Chisholm MH, Gama GJ, DiStasi VF, Hector AL, Parkin IP (1996) Molecular routes to metal carbides, nitrides, and oxides. 2. Studies of the ammonolysis of metal dialkylamides and hexamethyldisilylamides. *Chem Mater* 8:1222–1228
- [29] Bradley DC, Hursthouse MB, Malik KMA, Moseler R (1978) The crystal molecular structure of “bis(hexamethyldisilylamido) manganese”. *Transit Metal Chem* 3:253–254
- [30] Fröhling B, Kreiner G, Jacobs H (1999) Synthese und kristallstruktur von mangan(II)- und zinkamid,  $Mn(NH_2)_2$  und  $Zn(NH_2)_2$ . *Z Anorg Allg Chem* 625:211–216
- [31] Bergstrom FW (1924) Potassium ammono-aluminate, potassium ammonomanganite and manganous amide. *J Am Chem Soc* 46:1545–1558
- [32] Yarema M, Caputo R, Kovalenko MV (2013) Precision synthesis of colloidal inorganic nanocrystals using metal and metalloid amides. *Nanoscale* 5:8398–8410
- [33] Janik JF, Wells RL (1996) Gallium imide,  $\{Ga(NH)_3/2\}_n$ , a new polymeric precursor for gallium nitride powders. *Chem Mater* 8:2708–2711
- [34] Wells RL, Janik JF, Gladfelter WL, Coffey JL, Johnson MA, Steffey BD (1997) New precursor routes to nanocrystalline cubic/hexagonal gallium nitride, GaN. *Mater Res Soc Symp Proc* 468:39–45
- [35] Drygaś M, Olejniczak Z, Grzanka E, Bućko MM, Paine RT, Janik JF (2008) Probing the structural/electronic diversity

- and thermal stability of various nanocrystalline powders of gallium nitride GaN. *Chem Mater* 20:6816–6828
- [36] Janik JF, Wells RL, Coffey JL, John JVSt, Pennington WT, Schimek GL (1998) Nanocrystalline aluminum nitride and aluminum/gallium nitride nanocomposites via transamination of  $[M(NMe_2)_3]_2$ ,  $M = Al, Al/Ga$  (1/1). *Chem Mater* 10:1613–1622
- [37] Grzanka E, Stelmakh S, Palosz B, Gierlotka S, Proffen T, Drygaś M, Janik JF (2011) Core-shell structure of nanocrystalline AlN in real and reciprocal spaces. *Z Kristallogr Proc* 1:235–240
- [38] Drygaś M, Czosnek C, Janik JF (2006) Book of abstracts of *NANOMAT 2006 – international workshop on nanostructured materials*. Antalya, June 21–23, pp 201
- [39] Stelmakh S, Grzanka E, Gierlotka S, Janik JF, Drygaś M, Lathe C, Palosz B (2011) Compression and thermal expansion of nanocrystalline TiN. *Z Kristallogr Proc* 1:241–246
- [40] Andersen RA, Faegri KJr, Green JC, Haaland A, Lappert MF, Leung WP, Rypdal K (1988) Synthesis of bis[bis(trimethylsilyl)amido]iron(II). Structure and bonding in  $M[N(SiMe_3)_2]_2$  ( $M =$  manganese, iron, cobalt): two-coordinate transition-metal amides. *Inorg Chem* 27:1782–1786
- [41] Olmstead MM, Power PP, Shoner SC (1991) Three-coordinate iron complexes. *Inorg Chem* 30:2547–2551
- [42] Baxter DV, Chisholm MH, Gama GJ, Hector AL, Parkin IP (1995) Low pressure chemical vapor deposition of metallic films of iron, manganese, cobalt, copper, germanium and tin employing bis(trimethyl)silylamido complexes,  $M(N(SiMe_3)_2)_n$ . *Chem Vapor Depos* 1:49–51
- [43] Maya L (1986) Synthetic approach to aluminum nitride via pyrolysis of a precursor. *Adv Ceram Mater* 1:150–153
- [44] Hector AL, Parkin IP (1995) Magnesium and calcium nitrides as nitrogen sources in metathetical reactions to produce metal nitrides. *Chem Mater* 7:1728–1733